Journal of Geography and Cartography (2023) Volume 6 Issue 1
doi:10.24924/jgc.v6i1.2184

ORIGINAL RESEARCH ARTICLE

Comparative study of sediment loading in sub-watersheds of Phewa Lake, Nepal

Bikesh Jojiju*, Rajan Subedi

Institute of Forestry, Pokhara Campus, Tribhuvan University, Pokhara 33700, Nepal. E-mail: jojiju-bikesh8@gmail.com

ABSTRACT

The present study assessed the potential of sediment loading in Beteni, Lauruk, Andheri, and Harpan sub-watersheds of Phewa Lake and estimated the sediment yield in the year 2020. Morphometry, land use/land cover, geology, climate, and human and development factors of the sub-watersheds were studied to assess the potential of sediment loading in the sub-watersheds. SRTM DEM was used for the computation of morphometric parameters and land use/land cover maps were prepared by using Landsat imagery. Geology, rainfall data, census data, and road maps were collected from various secondary sources. The sediment yields of the four sub-watersheds in the year 2020 were estimated by measuring the sediment volume deposited in the sediment retention ponds at the outlet of each sub-watershed. Results indicated that Beteni had the highest potential for sediment loading, while Harpan had the lowest. Likewise, the sediment yields for Beteni, Lauruk, Andheri, and Harpan sub-watersheds in 2020 were estimated at 1,420.67 m^3/km^2/year, 2,280.14 m^3/km^2/year, 1,666.77 m^3/km^2/year, and 766.42 m^3/km^2/year, respectively. To reduce sedimentation in Phewa Lake, it is recommended to regularly maintain siltation dams and construct check dams along the drainage slopes, alongside other soil conservation measures and appropriate land use practices in the upstream areas of the sub-watersheds.

Keywords: Phewa Watershed; Siltation Dam; Sediment Yield; Morphometric Analysis; Land Use/Land Cover

ARTICLE INFO

Received: 23 April 2023
Accepted: 30 May 2023
Available online: 15 June 2023

1. Introduction

Sediments are soil and rock fragments suspended, transported, and deposited by flowing water[1]. Sediments originate from erosion of soil, weathering of rocks, and mass movements such as landslides and debris flows[2]. Sediment transfer is affected by natural factors such as temperature and precipitation and anthropogenic factors including population and land use type of the basin. River sediment transfer is one of the major problems worldwide. Soil erosion and sedimentation have an impact on agriculture, reservoirs and lakes, and aquatic biodiversity. Sediment removal through erosion (on-site effects) leads to its transport and subsequent deposition in distant areas, including potentially fertile agricultural lands (off-site effects). The off-site effects of sedimentation also include siltation, which raises riverbed elevation[3], increases the risk of flooding in low-lying areas and poses threats to human lives[4].

Sediment yield is the consequence of erosion and deposition processes and depends on all those factors that affect erosion and sediment delivery[5]. Soil erosion and sediment delivery depends on climate[6–9], soil[10,11], vegetation cover[8,9,12], basin morphometry[12,13], land use[6,7,14–16], and socio-economic factors[17,18]. Amount, intensity, and frequency of rainfall influence runoff, which in turn affects soil erosion and

sediment yield. Several studies have shown that the sedimentation rate increases with an increase in rainfall intensity[19,20]. Likewise, land use/land cover is also seen as the key driver of sediment dynamics globally. Forest has higher water percolation, reduced surface runoff, and less sediment yield, whereas agricultural land has comparatively higher sediment yield[21]. Infrastructure development, such as road construction, cause slope instability if not properly managed. The surfaces of rural roads contain a high proportion of fine materials that are easily erodible, have low infiltration rates[22], have a high runoff, and generate a high sediment load[23–25]. Similarly, mass movements like landslides and gully erosion are frequent on poorly designed and poorly paced roads that deliver sediment to the streams[26–28]. Morphometric parameters of watersheds are another crucial factors that influence sediment loading. Several studies have established a significant correlation between these parameters and sediment transport processes. For instance, larger watershed areas contribute to higher sediment loading due to the accumulation of more sediment from erosion sources, however, the sediment yield decreases for larger watersheds due to a decrease in slope gradient[29]. Similarly, the shape of the watershed, characterized by parameters such as elongation ratio, circularity ratio, and form factor, also influences sediment loading[30]. Furthermore, the slope of the watershed also plays a crucial role, as steeper slope results in intensified soil erosion and sediment transport[31–33].

Various methods have been employed worldwide for the estimation of sediment yield, incorporating both field measurements and modeling approaches. One commonly used method is the sediment rating curve which establishes a relationship between stream discharge and sediment concentration. This method has been widely employed in hydrological studies, for instance, by Boukhrissa *et al.*[34], Wu *et al.*[35], Zhang *et al.*[36], and Sedighi *et al.*[37]. Hydrological models can also be used for the assessment and prediction of sediment yield from watersheds. These models use various information such as precipitation, land use practices, soil type, and topography as inputs for the simulation of the models[38]. For example, Serrão *et al.*[39] used Soil and Water Assessment Tool (SWAT) to investigate the sediment yield of a basin in the Brazilian Amazon. Likewise, Admas *et al.*[40] used the geospatial Water Erosion Prediction Project (WEPP) to model sediment yield Megech Watershed of the upper Blue Nile Basin. A bathymetric survey of reservoirs is another method for determining sediment yield. This method involves comparing the initial sediment level with the present sediment level to estimate reservoir sedimentation[41]. Endalew and Mulu[42] used the bathymetric survey to estimate reservoir sedimentation at the Shumburit earth dam in Ethiopia.

Phewa Lake, the second largest lake in Nepal, is a stream-fed, dam-regulated semi-natural freshwater lake[43] situated in the southwestern part of Pokhara Metropolitan City. The lake provides significant ecosystem services to the local community including tourism, hydroelectricity, irrigation, fishing, boating, and its natural beauty[44,45]. However, the condition of the lake is deteriorating, thereby affecting the supply of ecosystem services to the local residents. Several issues are existing in the lake that impacts the health of Phewa Lake including lake area encroachment, sedimentation, water pollution, eutrophication, invasive species, toxic contamination, unmanaged fishing, acidification, and climate changes[46–48]. The area of Phewa Lake was 10 km^2 in 1956/57 which was reduced to 4.4 km^2 by 1998[49], which further reduced to 4.02 km^2 in 2019[50] thus losing about 60% of its area over seven decades. Several studies have been conducted over the years to estimate the annual sediment accumulation in Phewa Lake and its potential impact on the lake's capacity. In 1994, the survey conducted by the Department of Soil Conservation estimated that the annual sediment accumulation in Phewa Lake was between 175,000 and 225,000 m^3[51]. However, subsequent research conducted by Ross and Gilbert in 1995–1996 revealed a significant decrease, with an estimated sediment accumulation of 78,700 m^3 and anticipated that the lake will lose 80% of its capacity within 360 years (by 2359)[52]. Sthapit and Balla conducted a survey covering the period from March 1990 to February 1998, which revealed an annual sedimentation rate of approximately 180,000 m^3/year. They concluded that if this sedimentation rate persisted,

Phewa Lake would lose 80% of its storage capacity within the next 190 years (by 2188), rendering the lake practically useless[53]. Furthermore, Watson *et al.*[50] estimated an annual sedimentation influx ranging from 79,000 m^3 to 224,000 m^3 in Phewa Lake. Their findings suggested that, at this rate, the lake would experience an 80% reduction in storage capacity within the next 110 to 347 years. The researchers attributed the high sedimentation levels in Phewa Lake to extensive river bank erosion, which was exacerbated by extreme rainfall and intensive land use practices without adequate soil conservation measures.

The issue of sedimentation should be addressed to conserve Phewa Lake. To mitigate sedimentation, siltation dams, and sediment retention ponds were constructed at the outlets of four streams of the Phewa watershed: Beteni Stream, Lauruk Stream, Andheri Stream, and Harpan Stream. These particular sub-watersheds, namely Beteni, Lauruk, Andheri, and Harpan, are not only the most vulnerable within the Phewa watershed but also the primary contributors to sediment loading into the Phewa Lake[46,54]. This construction initiative, led by the Gandaki Province Government and Pokhara Metropolitan Municipality, was completed at the beginning of 2020, prior to the monsoon season. However, an essential aspect of the project, the characterization of the sub-watershed and quantification of annual sediment deposition in the sediment retention pond, remains unexplored. Therefore, this study aimed to bridge the aforementioned research gap by conducting a comprehensive analysis of the sediment potential within the four sub-watersheds. This analysis included examining morphometry, land use/land cover, climate, and geology, as well as human and development factors. Additionally, the study aimed to estimate the sediment yield from these sub-watersheds specifically for the year 2020. The findings from this research will provide valuable insights for prioritizing sub-watersheds in the Phewa watershed and formulating effective conservation and watershed management strategies. Furthermore, the sediment yield data obtained for 2020 will serve as a baseline for future comparisons, enabling the assessment of changes in sediment yield within the sub-watersheds over time. Ultimately, the outcomes of this study will contribute to addressing the persistent problem of sedimentation in Phewa Lake and the Phewa watershed, facilitating their conservation and management.

2. Study area

Phewa watershed lies in the western part of Pokhara Valley of Kaski district in the Gandaki Province of Nepal. The watershed lies within the latitude of 28°11'40.15" to 28°17'25.95" north and longitude of 83°47'54.22" to 83°59'15.62" east. It covers an area of 121.93 km^2 with a geometrical east-west length of 18.32 km and north-south width of 9.53 km (**Figure 1**). The altitude of the watershed ranges from 791 meters above sea level (m.a.s.l.) at the lake surface to 2,480 m.a.s.l. at the top of Panchase. The terrain of the watershed, in general, is rugged and comprised of several folds and steep-sloped hills with several streams and rivers among Harpan and Andheri are the major ones. The land use pattern of the Phewa watershed shows that most of the area of the watershed is covered by forest (54.1%) followed by agriculture (40%). Built-up areas, water bodies, and degraded land occupy 5.1%, 4.7%, and 1% of the watershed area respectively[44]. The climate of the Phewa watershed is based on annual rainfall events which bring more than two-thirds of the annual rainfall between June to September. The study was carried out in four sub-watersheds (SWs) of the Phewa watershed, namely SW, Lauruk SW, Andheri SW, and Harpan SW. The characteristics of the four SWs are described in **Table 1**.

Table 1. Characteristics of the four SWs of Phewa Lake

S.N.	Name of SW	Area (km^2)	Elevation range (m.a.s.l.)	Aspect
1	Beteni SW	6.77	803–1,784	South
2	Lauruk SW	3.65	818–1,738	South
3	Andheri SW	26.37	819–2,065	South
4	Harpan SW	30.63	824–2,480	North

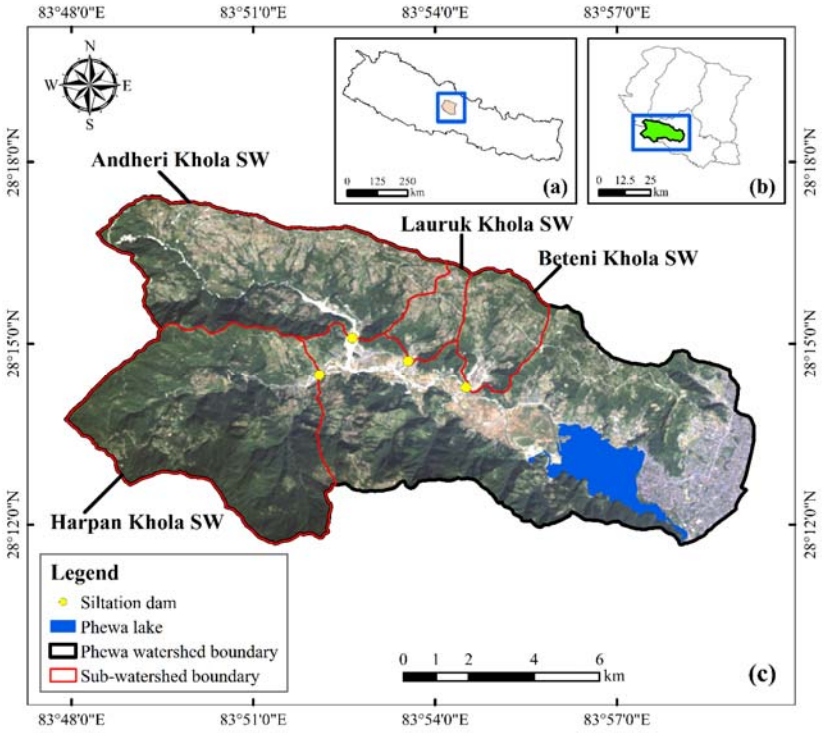

Figure 1. Map showing: (a) Kaski district within Nepal; (b) Phewa watershed within Kaski district; (c) Natural color composite of Landsat 8. (2.0.2.0.) clipped to Phewa watershed boundary.

3. Methodology

3.1 Data collection

The estimation of sediment volume deposited in the sediment retention pond of the four SWs was done through field observation and measurement. The length and breadth of the sediment retention pond were measured using a measuring tape. The level of sediment deposited in the pond was measured by systematic sampling of spot height using Pentax Total Station. A grid of 10 m by 10 m was laid on the pond using a measuring tape. At each point of the grid, GPS coordinates were taken and the sediment level was measured.

Training samples for the land use/land cover (LULC) classification were collected during field visits using GPS. Furthermore, the secondary data were also used in the study which were collected from different sources as illustrated in **Table 2**.

Table 2. Secondary data used in the study

Data	Year	Source
Landsat 8 satellite image resolution 30 m	2020	Google Earth Engine (GEE) repository
Shuttle radar topography mission (SRTM) digital elevation model (DEM) of resolution 30 m	-	United States Geological Survey (USGS) earth explorer website (https://earthexplorer.usgs.gov/)
Rainfall data (Pokhara Airport Station and Lumle Station)	1980 to 2020	Department of hydrology and meteorology
Road network	2020	Digitized from google earth imagery
Household and population data	2011	Central Bureau of Statistics
Geological map	-	Department of Mines and Geology

3.2 Data analysis

3.2.1 Estimation of sediment yield

The volume of sediment accumulated in the sediment retention pond was calculated by multiplying the average depth of the accumulated sediment by the pond area. The pond area is the length of the

pond times its breadth. The sediment yield of each SW was estimated by dividing the deposited sediment volume by the respective SW area.

3.2.2 Morphometric analysis

ArcGIS Hydrology tools were used for the delineation of SWs and stream networks from DEM. Siltation dams were taken as the outlets of the SWs. SWs boundaries and stream networks were converted to vector using a raster-to-vector conversion tool.

The SRTM DEM of 30 m resolution was used for the estimation of morphometric parameters of the four sub-watersheds. Spatial computations were done with the help of the ArcMap version 10.5. Microsoft Excel was used for the computations of some primary and derived morphometric parameters using attributes computed from spatial data. The morphometric parameters that were computed are stream order (*U*), stream number (*Nu*), stream length (*Lu*), mean stream length ($\bar{L}$), stream length ratio (*Rl*), bifurcation ratio (*Rb*), basin perimeter (*P*), basin length (*Lb*), basin area (*A*), drainage density (*Dd*), drainage texture (*T*), stream frequency (*Fs*), elongation ratio (*Re*), circularity ratio (*Rc*), form factor (*Ff*), relief (*R*), relief ratio (*Rf*), and Ruggedness number (*Rn*). The streams were ranked according to Strahler's stream ordering system[55]. **Table 3** explains the formulae used for the quantitative determination of the morphometric parameters.

Table 3. Formulae used for the computation of morphometric parameters

Morphometric parameters	Formula	References
Stream order (*U*)	Hierarchical order	[55]
Stream number (N_u)	$N_u = N_1 + N_2 + \ldots\ldots + N_n$	[56]
Stream length (L_u)	Length of the stream	[57]
Mean stream length ($\bar{L}$)	$\bar{L} = \sum L_u/N_u$, where, L_u = total stream length of order *u* and N_u = number of streams of order *u*	[57]
Stream length ratio (R_l)	$R_l = L_u/L_{u-1}$, where, L_u = total stream length of order *u* and L_{u-1} = total stream length of its next lower order	[57]
Bifurcation ratio (R_b)	$R_b = N_u/N_{u+1}$, where, N_u = number of streams of order *u* and N_{u+1} = number of streams of next higher order	[57]
Basin perimeter (*P*)	ArcGIS analysis	[58]
Basin length (L_b)	ArcGIS analysis	[58]
Basin area (*A*)	ArcGIS analysis	[58]
Drainage density (D_d)	$D_d = \sum L/A$, where, *L* = total length of stream and *A* = basin area	[59]
Drainage texture (*T*)	$T = \sum N/P$, where, *N* = total number of streams and *P* = basin perimeter	[56]
Stream frequency (F_s)	$F_s = \sum N/A$, where, *N* = total number of stream and *A* = basin area	[59]
Elongation ratio (R_e)	$R_e = (2/L_b)\sqrt{A/\pi}$, where, L_b = basin length, *A* = basin area and π = 3.14	[58]
Circularity ratio (R_c)	$R_c = 4\pi A/P^2$, where, *A* = basin area, π = 3.14 and *P* = basin perimeter	[57]
Form factor (F_f)	$F_f = A/L^2$, where, A = basin area and L = basin length	[59]
Relief (*R*)	$R = H - h$, where, *H* = maximum basin elevation and *h* = minimum basin elevation	[60]
Relief ratio (R_f)	$R_f = R/L$, where, *R* = basin relief and *L* = basin length	[61]
Ruggedness number (R_n)	$R_n = R \times D_d$, where, *R* = basin relief and D_d = drainage density	[61]

3.2.3 LULC analysis

Information regarding LULC is important for the land processes including hydrological and climatic processes. The LULC maps of respective sub-watersheds were generated using the cloud-based computing platform Google Earth Engine (GEE). Customized GEE code editors were used. LULC classification was done using pixel-based supervised classification with Machine Learning Algorithm (MLA). An examination of composite images was done to identify sets of training and testing polygons (based on images, Google Earth, and field visits) for

six classes (forest, agricultural land, water bodies, barren land, built-up area, and fan deposits) as Feature Collection using Geometric Tools and Import. These samples were used to train Random Forest (RF) classifier within the Google Earth Engine platform.

3.2.4 Climate analysis

Rainfall data from two stations in and around the Phewa watershed (Pokhara Airport Station and Lumle Station) from 1980 to 2020 were collected. Trend analysis of annual rainfall, number of rainfall days, and monsoon rainfall from 1980 to 2020 was done using Microsoft Excel.

3.2.5 Human and development factors

The population density of each sub-watershed was estimated from the census data of 2011. Ward population density (people/km^2) was calculated by dividing the ward population by ward area (km^2). Ward boundaries were mapped to the sub-watershed boundaries in ArcGIS. For each ward located only partially within the sub-watershed, it was assumed that the ward population density was uniform throughout the ward and the population was split in proportion to the ward area within the sub-watershed. The population density was then calculated by dividing the estimated sub-watershed population by the sub-watershed area. A similar method was used to calculate the household density (households/km^2) of each sub-watershed from the census data. The road density (km/km^2) of each sub-watershed was calculated by dividing the length of the road network (km) in that sub-watershed by its area (km^2).

4. Results and discussion

4.1 Natural factors affecting sediment yield

4.1.1 Morphometric parameters

Morphometric parameters such as linear aspects (stream order, stream number, steam length, mean stream length, bifurcation ratio, and mean bifurcation ratio), areal aspects (area, perimeter, basin length, drainage density, drainage texture, stream frequency, elongated ratio, circulatory ratio, and form factor) and relief aspect (basin relief, relief ratio, and ruggedness number) were computed. The morphometric parameters of the four SWs are tabulated in **Table 4**.

Table 4. Morphometric parameters of the four SWs

Morphometric parameters		Beteni SW	Lauruk SW	Andheri SW	Harpan SW
Stream number (N_u)	1	55	32	190	214
	2	18	7	43	50
	3	4	1	12	15
	4	1	-	3	4
	5	-	-	1	1
	Total	78	40	249	284
Stream length (L_u) km	1	19.55	10.79	57.70	61.43
	2	8.78	4.54	19.19	25.71
	3	2.70	1.59	10.26	10.16
	4	1.83	-	4.24	7.09
	5	-	-	3.43	4.30
	Total	32.86	16.91	94.81	108.69
Mean stream length ($\overline{L}$) km	1	0.36	0.34	0.30	0.29
	2	0.49	0.65	0.45	0.51
	3	0.68	1.59	0.85	0.68
	4	1.83	-	1.41	1.77
	5	-	-	3.43	4.30

Table 4. (*Continued*).

Morphometric parameters		Beteni SW	Lauruk SW	Andheri SW	Harpan SW
Stream length ratio (R_l)	2/1	0.45	0.42	0.33	0.42
	3/2	0.31	0.35	0.53	0.40
	4/3	0.68	-	0.41	0.70
	5/4	-	-	0.81	0.61
Bifurcation ratio (R_b)	R_{b1}	3.06	4.57	4.42	4.28
	R_{b2}	4.50	7.00	3.58	3.33
	R_{b3}	4.00	-	4.00	3.75
Bifurcation ratio (R_b)	R_{b4}	-	-	3.00	4.00
	Mean R_b	3.85	5.79	3.75	3.84
Area (A) km^2		6.77	3.65	26.37	30.63
Perimeter (P) km		10.94	8.98	24.81	24.48
Basin length (L_b) km		3.84	3.30	7.69	7.01
Drainage density (D_d) km/km^2		4.86	4.63	3.59	3.55
Drainage texture (T) km^{-1}		7.13	4.45	10.04	11.60
Stream frequency (F_s) km^{-2}		11.53	10.95	9.44	9.27
Elongation ratio (R_e)		0.76	0.65	0.75	0.89
Circularity ratio (R_c)		0.71	0.57	0.54	0.64
Form factor (F_f)		0.46	0.34	0.45	0.62
Maximum elevation (H) m		1,784	1,738	2,065	2,480
Minimum elevation (h) m		803	818	819	824
Relief (R) m		981	920	1,246	1,656
Relief ratio (R_f)		0.26	0.28	0.16	0.24
Ruggedness number (R_n)		4.76	4.26	4.48	5.88

Beteni SW has up to the 4th order stream, Lauruk SW has up to the 3rd order stream, Andheri SW has up to the 5th order stream and Harpan SW has up to the 5th order stream. The stream order is directly proportional to the watershed size. Since Harpan SW has a greater size, it also has a greater number of streams than the other SWs. Higher stream order is related to higher discharge and greater velocity of streamflow[57]. This implies that Andheri SW and Harpan SW have higher discharge and velocity of streamflow whereas Lauruk SW has lower discharge. The result also showed that the total stream length of the SWs is inversely proportional to the stream order. Similar results were reported by other empirical studies[62–65]. This is related to the slope and physiographic characteristics of the watershed. This further indicates that the infiltration capacity of the watershed varies with the level of stream order. A shorter stream length indicates steep slopes and a longer stream length indicates gentle slopes[66]. The drainage network maps of the SWs are illustrated in **Figure 2**.

The bifurcation ratio associates the hydrological characteristics of the watershed with its climatic condition and geological structure[65]. If the bifurcation ratio of a watershed is less than 3.0, the geological structure of the watershed is flat and homogeneous. Similarly, if the bifurcation ratio of the watershed lies between 3.0 and 5.0, the geological structure of the watershed does not affect its drainage pattern[57]. The bifurcation ratio of all four SW ranges between 3.0 to 5.0. It implies that the SWs have uneven topographic structures. The mean bifurcation ratio of Lauruk SW is higher than the other SWs, so it has a greater probability of flooding leading to greater sediment yield.

Low drainage density is found where basin relief is low and high drainage density is found where basin relief is high with high runoff and erosion potential[56,57]. With this regard, Beteni SW is relatively

more susceptible to higher sediment yield as it has a higher drainage density. Contrary to this, Harpan SW has the lowest drainage density and shall produce less sediment yield.

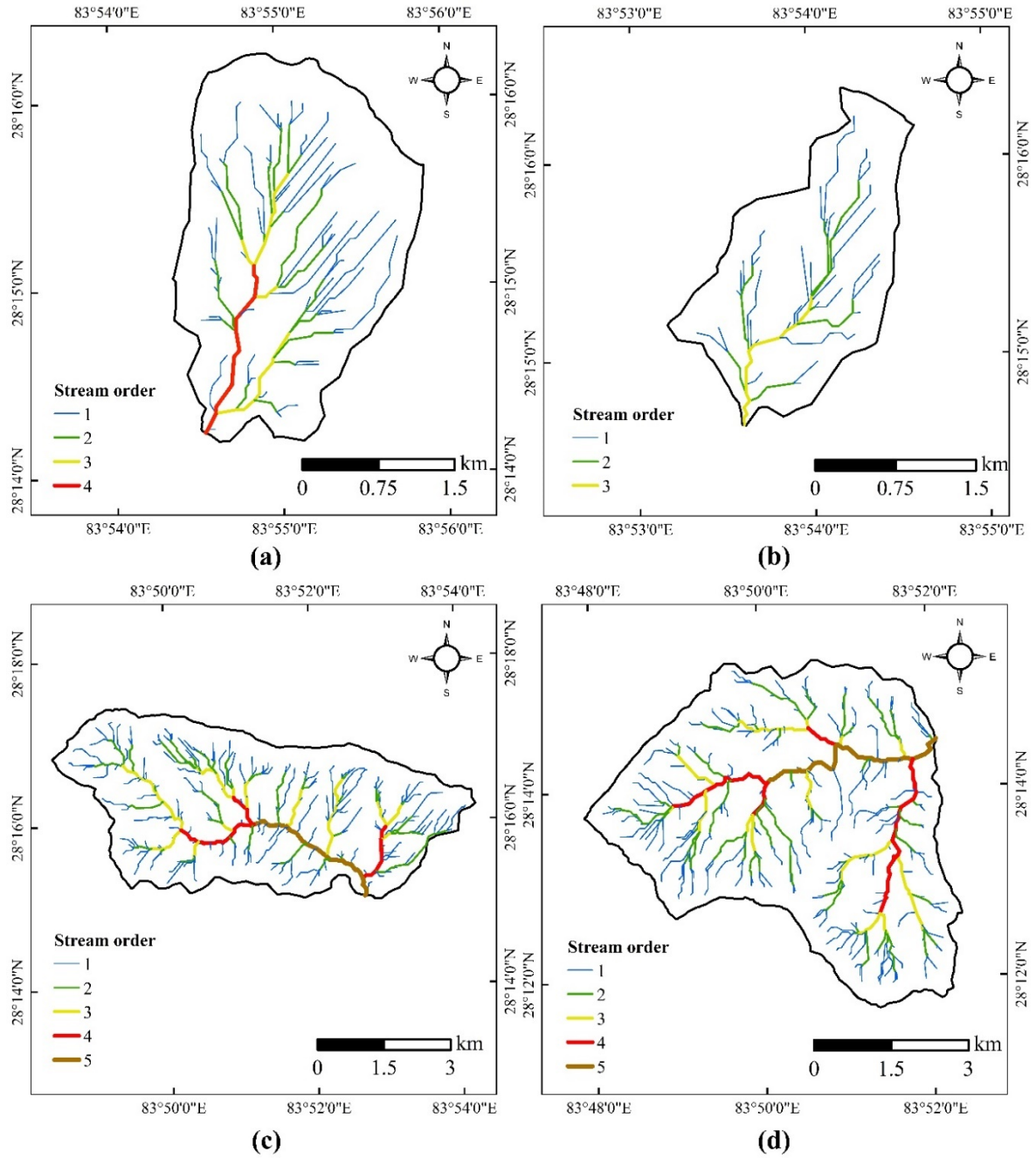

Figure 2. Drainage pattern and stream orders of (a) Beteni SW; (b) Lauruk SW; (c) Andheri SW; and (d) Harpan SW.

4.1.2 Slope

The slope map of the four SWs prepared using SRTM DEM is shown in **Figure 3**. The slope of Beteni SW varies from 0° to 46.70° with a mean slope of 20.81° and slope standard deviation of 7.03°. The slope of Lauruk SW varies from 0° to 48.49° with a mean slope of 18.24° and slope standard deviation of 6.40°. The slope of Andheri SW varies from 0° to 62.28° with a mean slope of 20.81° and slope standard deviation of 8.56°. The slope of Harpan SW varies from 0° to 58.85° with a mean slope of 22.74° and slope standard deviation of 9.10°. The higher average slope of the SWs is an indication of the generation of quick runoff during rainfall events. Harpan SW has the highest mean slope whereas Lauruk SW has the lowest mean slope.

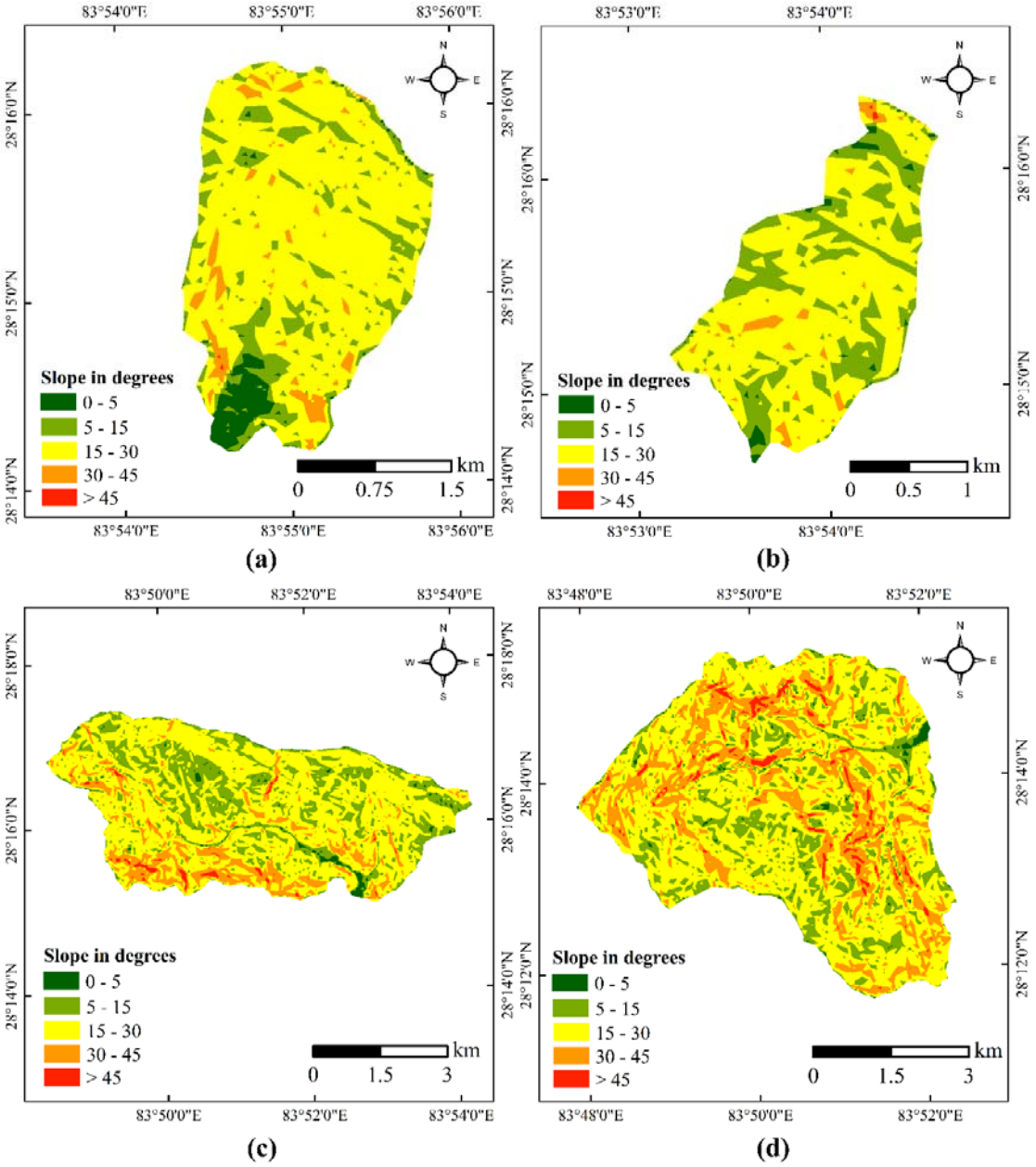

Figure 3. Slope distribution map of (a) Beteni SW, (b) Lauruk SW, (c) Andheri SW, and (d) Harpan SW.

Table 5. Distribution of slope classes in the four SWs

Slope class	Beteni SW		Lauruk SW		Andheri SW		Harpan SW	
	Area (km^2)	Area %	Area (km^2)	Area %	Area (km^2)	Area %	Area (km^2)	Area %
0°–5°	0.33	4.87	0.06	1.64	0.37	1.40	0.29	0.93
15°–30°	1.11	16.43	1.02	27.78	6.12	23.21	4.82	15.74
15°–30°	4.97	73.53	2.46	67.37	16.29	61.76	17.78	58.06
30°–45°	0.35	5.13	0.11	3.13	3.34	12.65	6.93	22.63
>45°	0.00	0.03	0.00	0.08	0.26	0.98	0.81	2.64

Slope-area analysis as shown in **Table 5** indicates that the maximum area of all the SW lies under a moderate slope (15°–30°). Harpan SW has larger areas under higher slopes (greater than 30°) than the other SWs. This also indicates that Harpan SW produces greater runoff during rainfall events. Therefore,

it is more prone to sediment loading than the other SWs.

4.1.3 Land use/land cover

The land use/land cover classes delineated for the four SWs include agricultural land, forest, built-up areas, water bodies, barren land, and fan deposits as shown in **Figure 4**. Beteni SW had 45.47%, 10.97%, 0.96%, 35.35%, and 7.15% under agricultural land, barren land, fan deposits, forest, and built-up area respectively. Lauruk SW had 55.25%, 7.81%, 0.63%, 30.19%, and 5.86% under agricultural land, barren land, fan deposits, forest, and built-up area, respectively. Andheri SW had 40.70%, 7.81%, 3.07, 44.97%, and 3.45% under agricultural land, barren land, fan deposits, forest, and built-up area respectively. Harpan SW had 13.97%, 2.13%, 0.26%, 82.54%, and 1.10% under agricultural land, barren land, fan deposits, forest, and built-up area respectively. These results show that Beteni SW

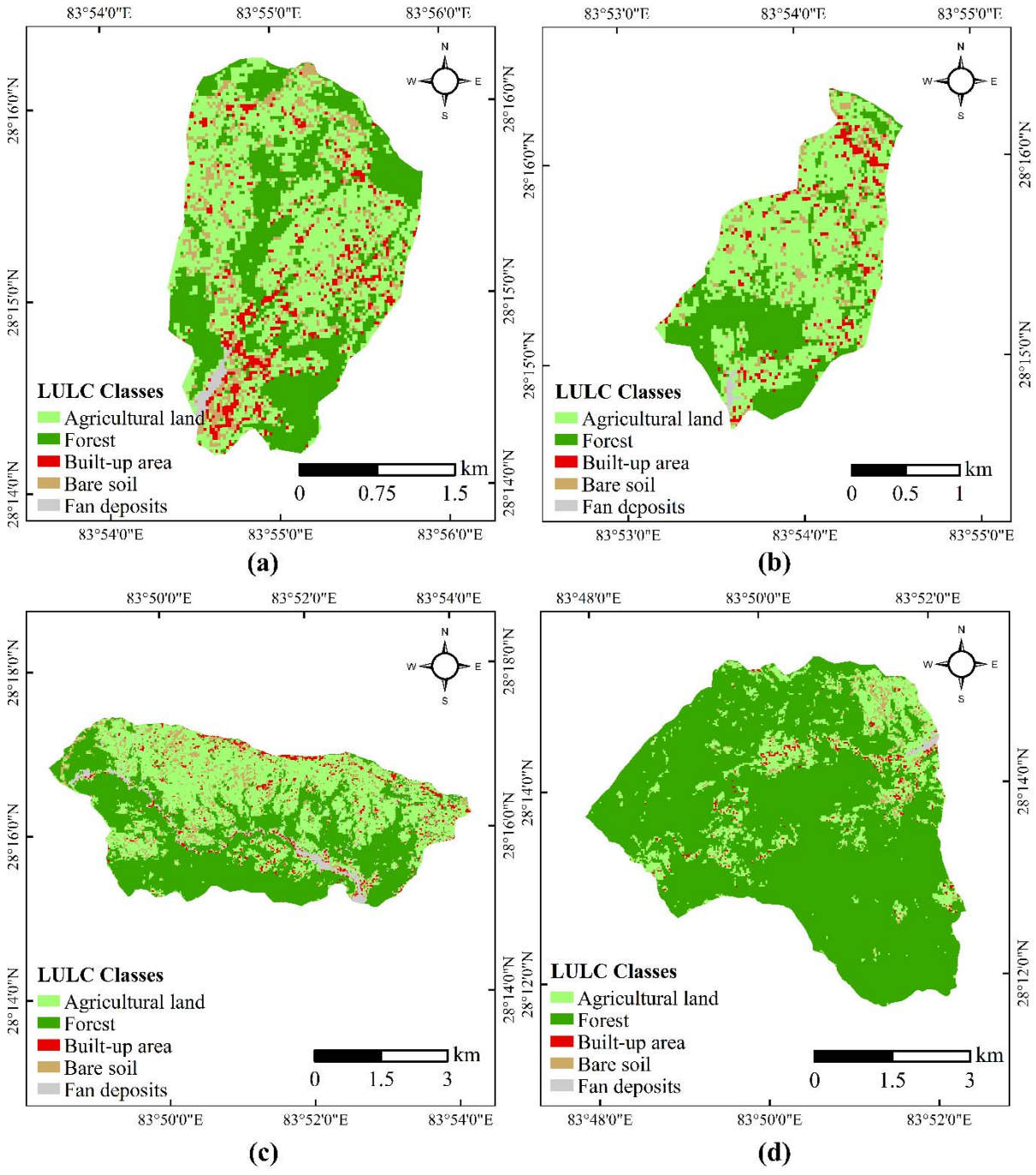

Figure 4. Land use land cover map of (a) Beteni SW; (b) Lauruk SW; (c) Andheri SW; and (d) Harpan SW.

and Lauruk SW were mostly covered by agricultural land while Andheri SW and Harpan SW had the highest percentage of forest area.

Beteni SW and Lauruk SW had less forest cover and more agricultural land as compared to Harpan SW. Similar results were shown by other studies[67,68]. Baral *et al.*[67] found that forest was dominant on the southern part and upper slopes and agricultural land and built-up area were more prevalent on valley floors, foot slopes, and hill terraces of the Phewa watershed.

The type and distribution of land use land cover classes have a high impact on hydrological processes[69]. Therefore, Beteni SW and Lauruk SW can generate more surface runoff as it has less forest cover compared to Andheri SW and Harpan SW. Harpan SW has most of the area covered by forest and shall produce less surface runoff and less sediment yield.

The distribution of agricultural land in different slope classes is depicted in **Figure 5**. Agricultural land was dominant in the moderate slope class (15°–30°). Similar results were shown by Leibundgut *et al.*[48]. The main reason for the dominance of agricultural land in this slope class was due to soil conditions, better ability for terracing, water drainage, and access to roads. Beteni SW, Lauruk SW, Andheri SW, and Harpan SW had 74.37%, 64.33%, 62.85%, and 55.55% of the agricultural land under moderate slope class (15°–30°), respectively. Similarly, 2.83%, 2.01%, 3.76%, and 14.77% of the agricultural land in Beteni SW, Lauruk SW, Andheri SW, and Harpan SW were above 30° slope.

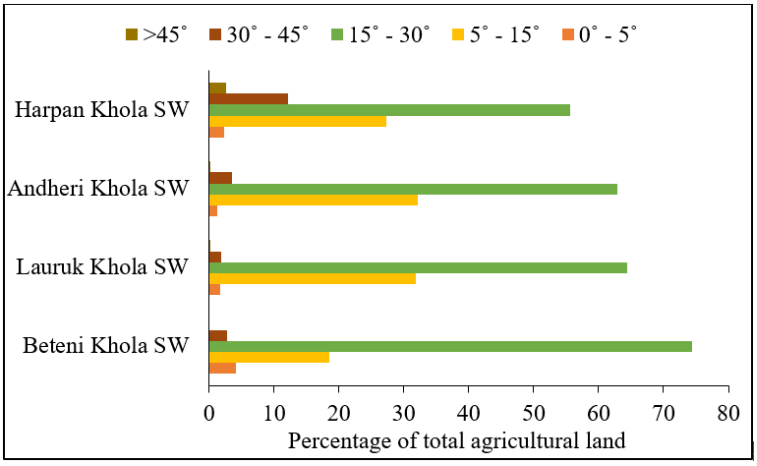

Figure 5. Distribution of agricultural land in different slope classes.

4.1.4 Geology

The Phewa watershed mostly comprises rocks of two formations; the Kuncha formation and the Fagfog quartzite of Central Nepal Lesser Himalaya. Kuncha Formation occupies the maximum area of Beteni SW, Lauruk SW, and Andheri SW whereas most of the area of Harpan is covered by Fagfog quartzite (**Figure 6**). Kuncha Formation occupies 87.84%, 80.01%, 57.05%, and 6.41% of Beteni SW, Lauruk SW, Andheri SW, and Harpan SW respectively. Similarly, 75.90% of Harpan SW is covered by the Fagfog quartzite formation. Kuncha formation is characterized by thin-to-medium beds of grey phyllites and grey sandstones that are thinly foliated and highly weathered. Fagfog quartzite is represented by white, medium to thick beds of coarse-grained quartzites. The quartzites are marked by massive beds and current ripples. Sand gravels are found in hill slopes and unconsolidated sediments are found in alluvial fan deposits. There is also the presence of large-scale thrust faults and many small faults.

The phyllites of the Kuncha formation are geologically fragile and are more likely to fail during monsoons[46]. However, quartzites are more stable compared to phyllites and less likely to slope failure. Kuncha formation comprises the maximum area of Beteni SW, Lauruk SW, and Andheri SW. Fagfog

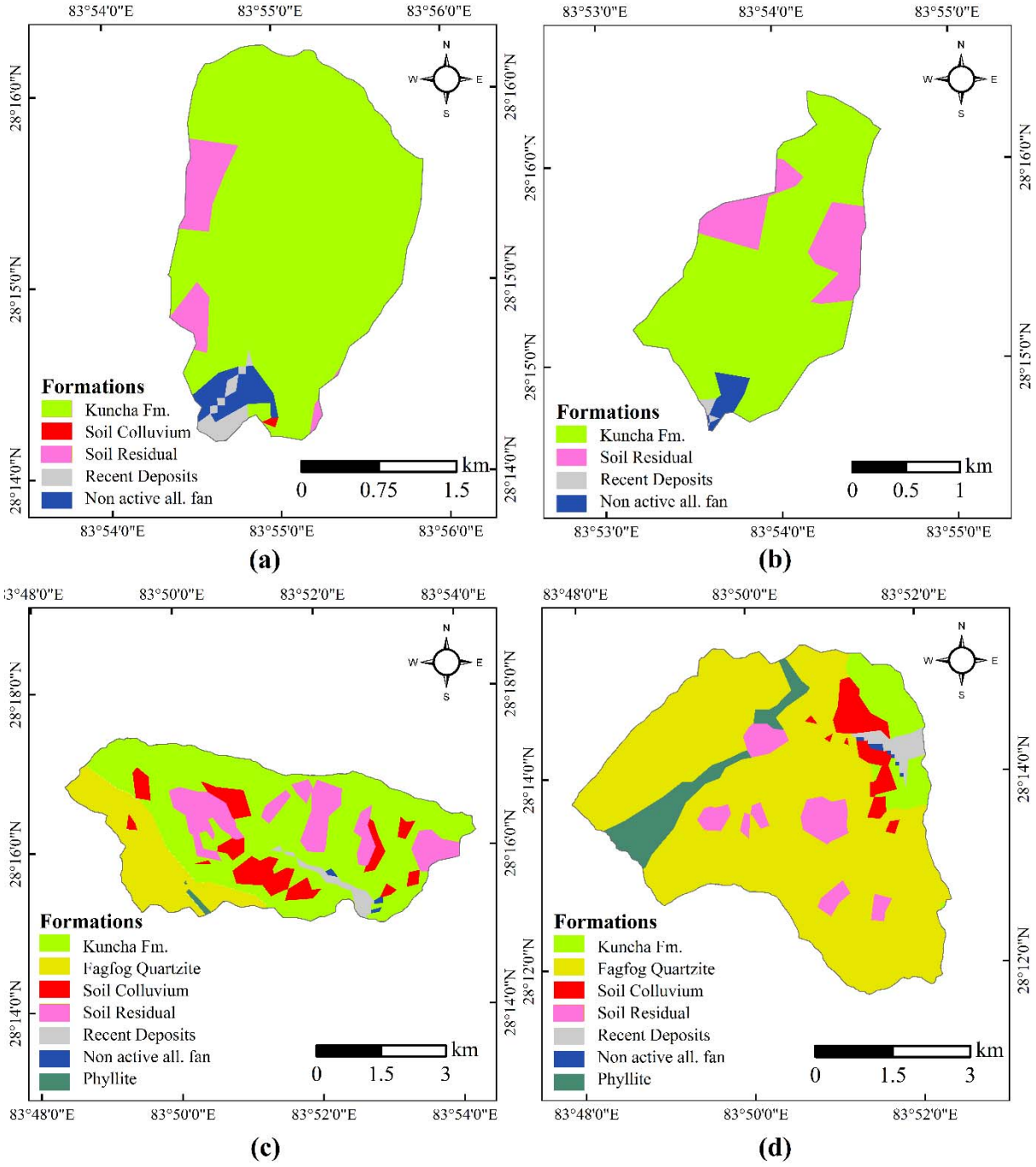

Figure 6. Geological map of (a) Beteni SW; (b) Lauruk SW; (c) Andheri SW; and (d) Harpan SW.

quartzites comprise the maximum area of Harpan SW. So, geologically, Harpan SW is more stable compared to Beteni SW, Lauruk SW, and Andheri SW. Due to stable geology, Harpan SW has less potential for sediment loading than other SWs.

4.1.5 Climate

The measured rainfall data at two stations in Kaski (Pokhara Airport Station and Lumle Station) from 1980 to 2020 were collected and analyzed. The rainfall amount varies intensively from year to year from 1980 to 2020. The linear trend was used to study the variations in the magnitude of rainfall at Pokhara Airport Station and Lumle Station. The trend of rainfall generally decreased at Pokhara station as shown in **Figure 7** and the mean annual precipitation was 3,838.66 mm. The highest rainfall recorded was 5,398.43 mm in the year 2020 and the lowest rainfall recorded was 2,966.8 mm in the year

2005. The analysis of rainfall amount at Lumle station showed a slightly increasing trend of annual rainfall from 1980 to 2020 with mean annual precipitation of 5,441.27 mm. The wettest year was 1995 with an annual rainfall of 6,556.7 mm while the lowest rainfall recorded was 4,294.7 mm in the year 2006.

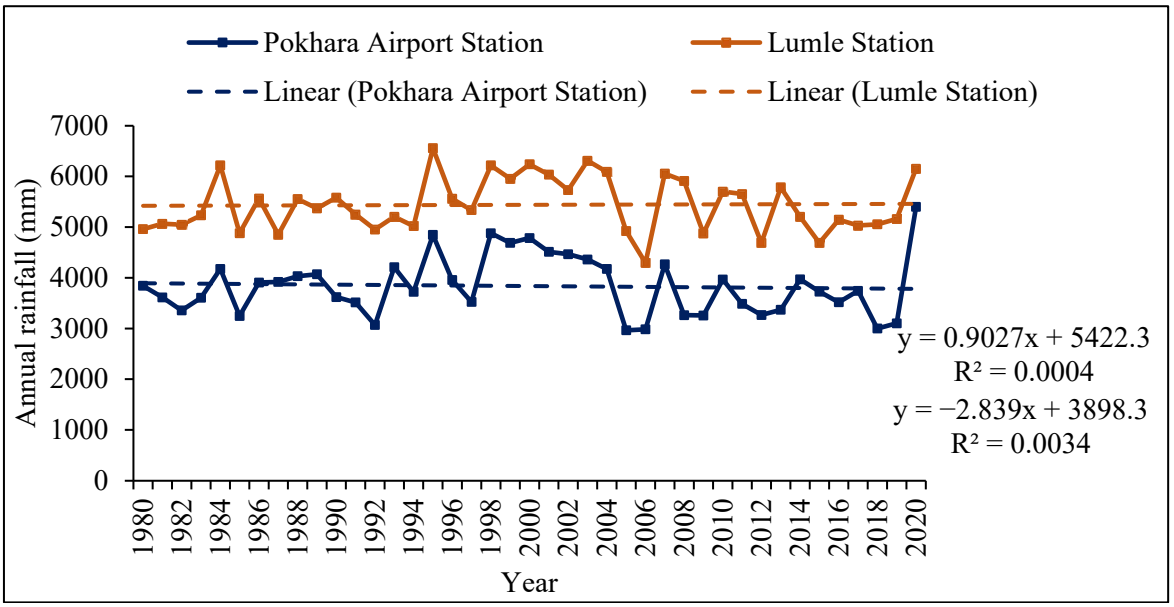

Figure 7. Trend analysis of annual rainfall from 1980 to 2020.

The annual rainfall in the year 2020 recorded at Pokhara Airport Station was 5,398.43 mm and at Lumle station was 6,152.23mm. Analysis of rainfall data shows a decrease in the number of rainfall days (**Figure 8**) and a corresponding increase in the number of dry days; however, the average annual rainfall is about the same. This means that the rainfall is more intensive within a shorter timeframe. The monsoon rainfall amount also varies intensively from year to year from 1980 to 2020. But the trend of monsoon rainfall is almost constant (**Figure 9**). The average monsoon rainfall at Pokhara station was 2,796.41 mm and at Lumle station was

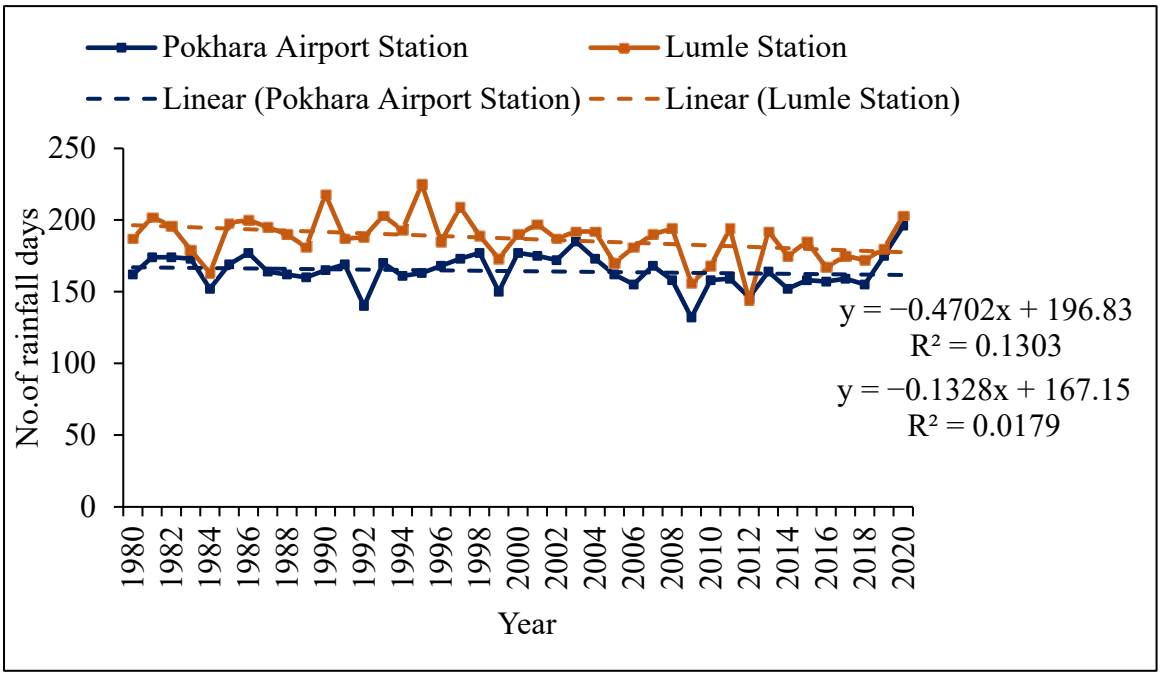

Figure 8. Trend analysis of the number of rainfall days from 1980 to 2020.

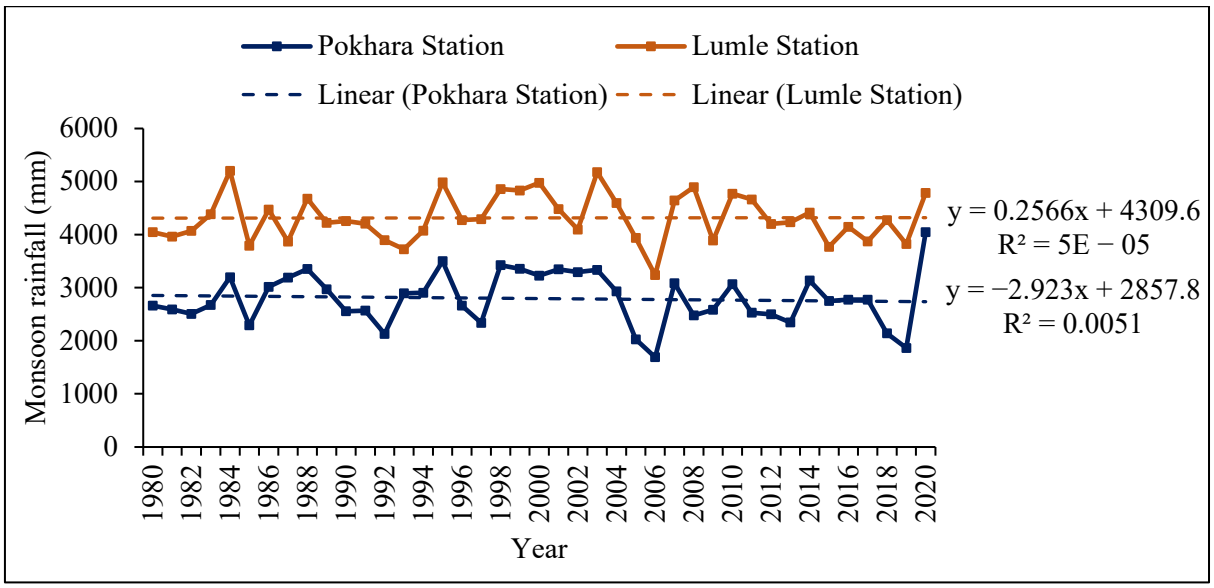

Figure 9. Trend analysis of monsoon rainfall from 1980 to 2020.

4,315.00 mm with about 76% of the rainfall occurring during monsoon.

The trend analysis of rainfall shows that the annual precipitation is slightly increasing but the number of rainfall days is decreasing. The annual rainfall in the year 2020 recorded at Pokhara Airport Station was 5,398.43 mm and at Lumle station was 6,152.23 mm. Annual rainfall and peak short-period rainfall amounts during extreme events could increase sediment delivery to Phewa Lake[50]. Frequent and intense rain events can increase erosion and result in greater amounts of sediment washing into rivers, lakes, and streams. Stronger storms, higher river levels, and faster stream velocity can increase erosion and result in increased suspended sediment (turbidity) in water bodies as well as affect the normal distribution of sediment along the river, lake, and stream beds.

4.2 Anthropogenic factors affecting sediment yield

4.2.1 Household density and population density

The household density of the SWs varied from 19 households/km^2 (in Andheri SW) to 82 households/km^2 (in Harpan SW) according to census 2011. This household density is much less as compared to the area around Phewa Lake. Watson *et al.* found that 505 buildings are located within 65 m and 1,687 buildings are located within 200 m distance from the shoreline of Phewa Lake in 2017[50]. The population density of SWs varied from 68 people/km^2 (in Harpan SW) to 321 people/km^2 (in Lauruk SW) according to the census 2011. The population of the Phewa watershed was 36,092 in 2001 which declined to 34,859 in 2011 but the number of households increased from 7,318 to 8,860[46]. This decrease in population might be due to the migration of people from higher elevations to lower elevations within the watershed as well as outmigration which is causing the abandonment of terrace farms. This has led to the failure of the terrace and gullies formation in many places leading to sedimentation into Phewa Lake[46]. The greater household density and population density of Lauruk SW suggest that it has a higher potential for sediment loading whereas Harpan has less potential for sediment loading. The population and household density maps of the SWs are illustrated in **Figures 10** and **11** respectively.

4.2.2 Road density

Beteni SW had the highest road density of 3.58 km/km^2 and Harpan had the lowest road density of 1.39 km/km^2. Similar results were shown by other studies[68]. The total road length of four SWs covering an area of 67.42 km^2 was 129.63 km in 2020 as digitized from Google Earth Imagery. The length of the rural earthen road in the Phewa watershed was 23 km in 1979 which was increased to 310 km in 2013[48] and 344 km in 2016[68]. An increase in rural earthen road networks increases road-induced sediment that contributes to the Phewa watershed sediment

budget[48]. Beteni SW and Lauruk SW have higher road density and can produce greater road indued sediment. The road network map of the SWs is given in **Figure 12**.

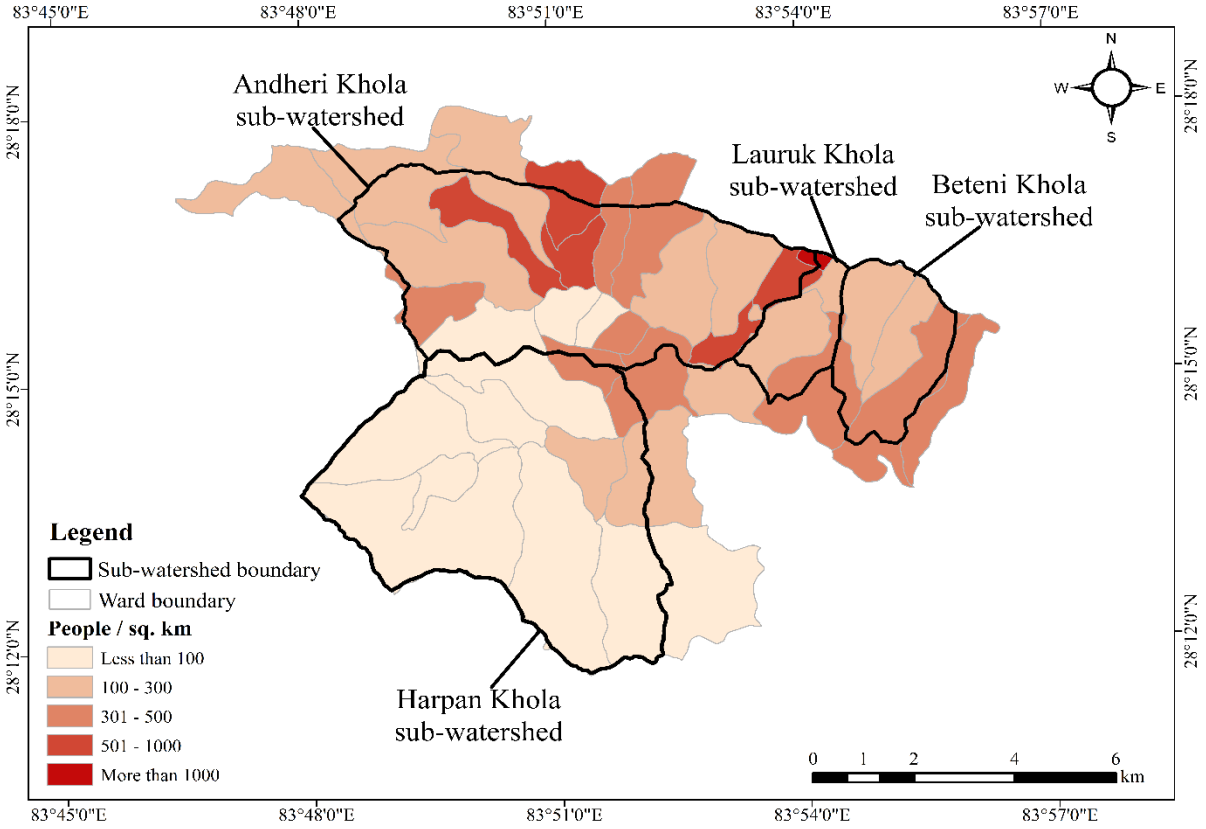

Figure 10. Population density maps of the four SWs.

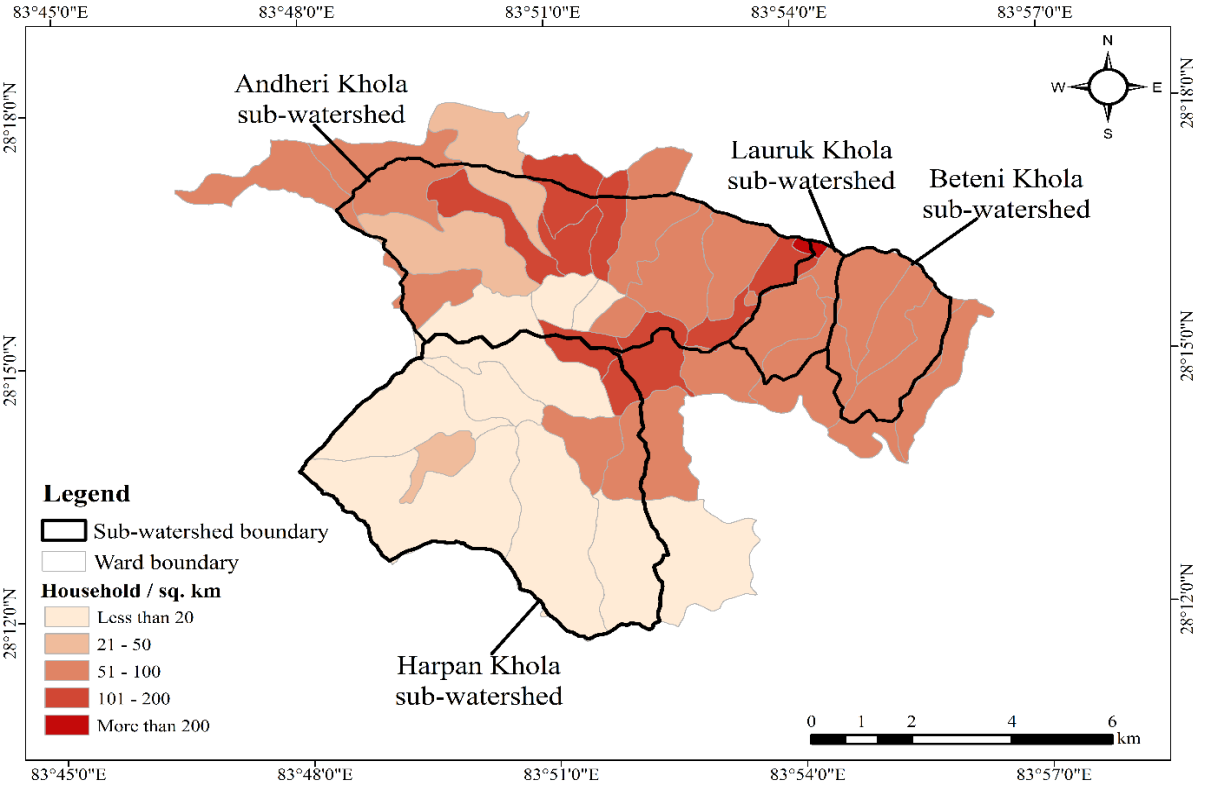

Figure 11. Household density map of the four SWs.

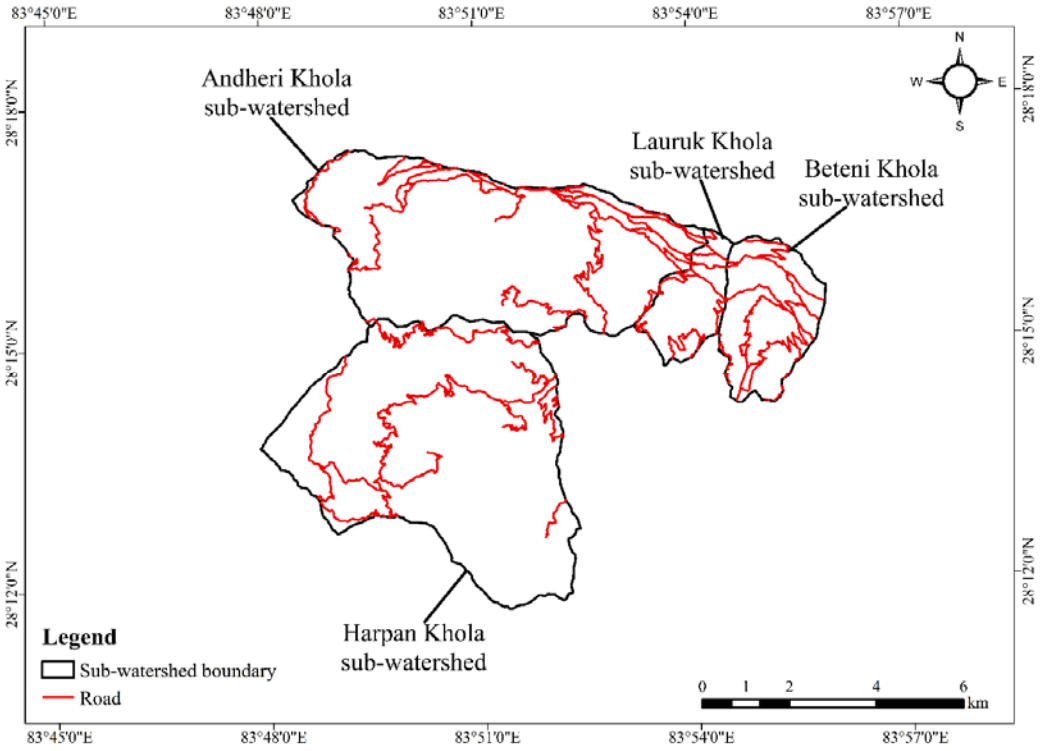

Figure 12. Road network of the four SWs.

4.3 Sediment yield of 2020

The sediment yield of the four SWs in the year 2020 is shown in **Figure 13**. The total deposited sediment volume in the four ponds was 85,368.45 m^3. The deposited sediment volume in the ponds of Beteni SW, Lauruk SW, Andheri SW, and Harpan SW was 9,617.92 m^3, 8,322.50 m^3, 43,952.63 m^3, and 23,475.40 m^3, respectively. The sediment yield of the sub-watersheds was estimated from the deposited sediment volume. The sediment yield of Lauruk SW was highest (2,280.14 m^3/km^2/year) followed by Andheri SW (1,666.47 m^3/km^2/year), Beteni SW (1,420.67 m^3/km^2/year), and Harpan SW (766.42 m^3/km^2/year). The high sediment yield at Lauruk SW in 2020 was due to intense agricultural practices in slopes and recent rural road construction activities.

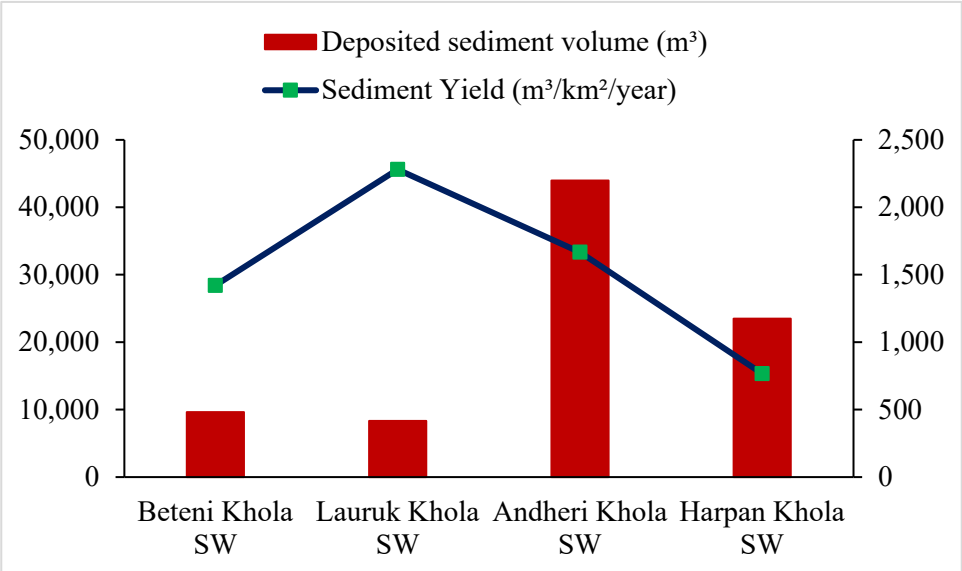

Figure 13. Sediment yield of the four SWs in 2020.

5. Conclusion

Phewa watershed lies in a fragile physiographic zone that experiences intense monsoon rainfall. In addition to natural processes, unplanned infrastructure development, and increasing population have triggered further destabilization of the land surface resulting in sedimentation into the Phewa Lake. By analyzing various factors such as morphometric parameters, LULC, geology, household density, population density, and road density, we have identified variations in sediment loading potential among the sub-watersheds. Harpan SW exhibits comparatively lower potential for sediment loading due to its lower drainage density, lower bifurcation ratio, greater forest cover, and stronger geology, coupled with lower household density, population density, and road density. On the other hand, Beteni SW displays a higher potential for sediment loading compared to the other sub-watersheds, attributable to its higher drainage density, higher bifurcation ratio, reduced forest cover, weaker geology, higher household density, population density, and road density. Regarding the sediment yield of the sub-watershed in 2020, Lauruk SW had the highest sediment yield at 2,280.14 m^3/km^2/year, while Harpan SW has the lowest at 766.42 m^3/km^2/year. Overall, the present study concludes that the study of morphometry, geology, LULC, climate, and human and development factors is vital to understand the sediment loading potential of a watershed. It is crucial to conduct appropriate land use planning and rural road construction by considering the local hydrogeology. Likewise, siltation dams and sediment retention ponds were found to be effective sediment-trapping structures at the outlets of the sub-watersheds. Even though the dams were successful to retain bedload and sand-gravel categories sediments, suspended sediments like mud and silt were allowed to flow through the dams, which were not assessed by the present study. Therefore, further estimation of suspended sediment should be done in the future to analyze the total sediment generated and transported within the sub-watersheds. Also, the capacity of retention ponds was less than the amount of sediment brought by the streams. So, it is advisable to remove the sediment deposited in the pond at least twice during monsoon to ensure maximum efficiency of the pond. The lifespan of the siltation dams was short and were likely to fail during heavy flood, i.e., to ensure their sustainability, they should be integrated with a series of check dams and bamboo plantation along the drainage and on-site soil conservation measures. Economic utilization of deposited materials in retention ponds, bamboo-based enterprise and commercial agroforestry system can offset the cost of conservation.

Author contributions

Conceptualization, BJ and RS; data collection and analysis, BJ; writing—original draft preparation, BJ; writing—review and editing, RS; supervision; RS.

Conflict of interest

The authors declare that there is no conflict of interest.

References

1. Hayter EJ, Gailani JZ. Fundamentals of sediment transport. In: Reible DD (editor). Processes, assessment and remediation of contaminated sediments. New York: Springer; 2014. Volume 6, p. 25–79.
2. Westrich B, Forstner U (editors). Sediment dynamics and pollutant mobility in rivers—An Interdisciplinary approach. Berlin: Springer; 2007.
3. Gunawan TA, Daud A, Haki H, Sarino. The estimation of total sediments load in river tributary for sustainable resources management. In: IOP conference series: Earth and environmental science, IOP Conference Series: Earth and Environmental Science; International Conference on SMART CITY Innovation 2018; 2018 Oct 25–26; Bandung, Indonesia. IOP Publishing; 2019. Volume 248, 012079.
4. Mahabaleshwara H, Nagabhushan HM. A study on soil erosion and its impacts on floods and sedimentation. International Journal of Research in Engineering and Technology 2014; 3(3): 443–451. doi: 10.15623/ijret.2014.0315086.
5. Dutta S. Soil erosion, sediment yield and sedimentation of reservoir: A review. Modeling Earth Systems and Environment 2016; 2(3): 1–18. doi: 10.1007/s40808-016-0182-y.
6. Borrelli P, Robinson DA, Panagos P, Ballabio C. Land use and climate change impacts on global soil erosion by water (2015–2070). Proceedings of the National Academy of Sciences of the United States of America 2020; 117(36): 21994–22001. doi: 10.1073/pnas.2001403117.
7. Bai Y, Ochuodho TO, Yang J. Impact of land use and climate change on water-related ecosystem services in Kentucky, USA. Ecological Indicators

2019; 102: 51–64. doi: 10.1016/j.ecolind.2019.01.079.
8. Zhao B, Zhang L, Xia Z, *et al.* Effects of rainfall intensity and vegetation cover on erosion characteristics of a soil containing rock fragments slope. Advances in Civil Engineering 2019; 2019: 1–14 doi: 10.1155/2019/7043428.
9. Zhang S, Li Z, Lin X, Zhang C. Assessment of climate change and associated vegetation cover change on watershed-scale runoff and sediment yield. Water 2019; 11(7): 1373. doi: 10.3390/w11071373.
10. Azimi Sardari MR, Bazrafshan O, Panagopoulos T, Rafiei Sardooi E. Modeling the impact of climate change and land use change scenarios on soil erosion at the Minab Dam watershed. Sustainability 2019; 11(12): 3353. doi: 10.3390/su11123353.
11. Chuenchum P, Xu M, Tang W. Estimation of soil erosion and sediment yield in the Lancang-Mekong River using the modified revised universal soil loss equation and GIS techniques. Water 2020; 12(1): 135. doi: 10.3390/w12010135.
12. Gao J, Jiang Y, Wang H, *et al.* Identification of dominant factors affecting soil erosion and water yield within ecological red line areas. Remote Sensing 2020; 12(3): 399. doi: 10.3390/rs12030399.
13. Sharma S, Mahajan AK. GIS-based sub-watershed prioritization through morphometric analysis in the outer Himalayan region of India. Applied Water Science 2020; 10(7): 1–11. doi: 10.1007/s13201-020-01243-x.
14. Ebabu K, Tsunekawa A, Haregeweyn N, *et al.* Effects of land use and sustainable land management practices on runoff and soil loss in the Upper Blue Nile basin, Ethiopia. Science of the Total Environment 2019; 648: 1462–1475. doi: 10.1016/j.scitotenv.2018.08.273.
15. Daramola J, Adepehin EJ, Ekhwan TM, *et al.* Impacts of land-use change, associated land-use area and runoff on watershed sediment yield: Implications from the Kaduna watershed. Water 2022; 14(3): 1–23. doi: 10.3390/w14030325.
16. Yaekob T, Tamene L, Gebrehiwot SG, *et al.* Assessing the impacts of different land uses and soil and water conservation interventions on runoff and sediment yield at different scales in the central highlands of Ethiopia. Renewable Agriculture and Food Systems 2022; 37: S73–S87. doi: 10.1017/S1742170520000010.
17. Zhong X, Jiang X, Li L, *et al.* The impact of socio-economic factors on sediment load: A case study of the yanhe river watershed. Sustainability 2020; 12(6): 2457. doi: 10.3390/su12062457.
18. Du J, Shi C, Fan X, Zhou Y. Impacts of socio-economic factors on sediment yield in the Upper Yangtze River. Journal of Geographical Sciences 2011; 21(2): 359–371. doi: 10.1007/s11442-011-0850-9.
19. Azari M, Moradi HR, Saghafian B, Faramarzi M. Climate change impacts on streamflow and sediment yield in the North of Iran. Hydrological Sciences Journal 2016; 61(1): 123–133. doi: 10.1080/02626667.2014.967695.
20. Li T, Gao Y. Runoff and sediment yield variations in response to precipitation changes: A case study of Xichuan watershed in the Loess Plateau, China. Water 2015; 7(10): 5638–5656. doi: 10.3390/w7105638.
21. Zhang L, Meng X, Wang H, Yang X. Simulated runoff and sediment yield responses to land-use change using the SWAT model in Northeast China. Water 2019; 11(5): 915. doi: 10.3390/w11050915.
22. Ziegler AD, Negishi JN, Sidle RC, *et al.* Persistence of road runoff generation in a logged catchment in Peninsular Malaysia. Earth Surface Processes and Landforms 2007; 32(13): 1947–1970. doi:10.1002/esp.1508.
23. Thomaz EL, Vestena LR, Ramos Scharrón CE. The effects of unpaved roads on suspended sediment concentration at varying spatial scales—A case study from Southern Brazil. Water and Environment Journal 2014; 28(4): 547–555. doi:10.1111/wej.12070.
24. Rijsdijk A, Sampurno Bruijnzeel LA, Sutoto CK. Runoff and sediment yield from rural roads, trails and settlements in the upper Konto catchment, East Java, Indonesia. Geomorphology 2007; 87(1–2): 28–37. doi:10.1016/j.geomorph.2006.06.040.
25. Lima Farias TR, Medeiros PHA, Navarro-Hevia J, Carlos de Araújo J. Unpaved rural roads as source areas of sediment in a watershed of the Brazilian semi-arid region. International Journal of Sediment Research 2019; 34(5): 475–485. doi: 10.1016/j.ijsrc.2019.03.002.
26. Egboka BC, Orji AE, Nwankwoala HO. Gully erosion and landslides in Southeastern Nigeria: Causes, consequences and control measures. Global Journal of Engineering Sciences 2019; 2(4): 1–11. doi: 10.33552/gjes.2019.02.000541.
27. MacDonald LH, Coe DBR. Road sediment production and delivery: Processes and management [Interent]. Available from: https://ucanr.edu/sites/forestry/files/138028.pdf.
28. Sidle RC, Furuichi T, Kono Y. Unprecedented rates of landslide and surface erosion along a newly constructed road in Yunnan, China. Natural Hazards 2011; 57(2): 313–326. doi: 10.1007/s11069-010-9614-6.
29. de Vente J, Poesen J, Arabkhedri M, Verstraeten G. The sediment delivery problem revisited. Progress in Physical Geography 2007; 31(2): 155–178. doi: 10.1177/0309133307076485.
30. Soni S. Assessment of morphometric characteristics of Chakrar watershed in Madhya Pradesh India using geospatial technique. Applied Water Science 2017; 7(5): 2089–2102. doi: 10.1007/s13201-016-0395-2.
31. Liu Y, Deng Z, Wang X. The effects of rainfall, soil type and slope on the processes and mechanisms of rainfall-induced shallow landslides. Applied Sciences 2021; 11(24): 11652. doi: 10.3390/app112411652.

32. Sime CH, Abebe WT. Sediment yield modeling and mapping of the spatial distribution of soil erosion-prone areas. Applied and Environmental Soil Science 2022; 2022. doi: 10.1155/2022/4291699.
33. Zhang K, Xuan W, Yikui B, Xiuquan X. Prediction of sediment transport capacity based on slope gradients and flow discharge. PLoS One 2021; 16(9): e0256872. doi: 10.1371/journal.pone.0256827.
34. Boukhrissa ZA, Khanchoul K, Le Bissonnais Y, Tourki M. Prediction of sediment load by sediment rating curve and neural network (ANN) in El Kebir catchment, Algeria. Journal of Earth System Science 2013; 122(5): 1303–1312. doi:10.1007/s12040-013-0347-2.
35. Wu C, Ji C, Shi B, *et al.* The impact of climate change and human activities on streamflow and sediment load in the Pearl River basin. International Journal of Sediment Research 2019; 34(4): 307–321. doi: 10.1016/j.ijsrc.2019.01.002.
36. Zhang F, Zeng C, Wang G, *et al.* Runoff and sediment yield in relation to precipitation, temperature and glaciers on the Tibetan Plateau. International Soil and Water Conservation Research 2022; 10(2): 197–207. doi: 10.1016/j.iswcr.2021.09.004.
37. Pronoos Sedighi M, Ramezani Y, Nazeri Tahroudi M, Taghian M. Joint frequency analysis of river flow rate and suspended sediment load using conditional density of copula functions. Acta Geophysica 2023; 71(1): 489–501. doi: 10.1007/s11600-022-00894-5.
38. Ijaz MA, Ashraf M, Hamid S, *et al.* Prediction of sediment yield in a data-scarce river catchment at the sub-basin scale using gridded precipitation datasets. Water 2022; 14(9): 1480. doi: 10.3390/w14091480.
39. Afonso de Oliveira Serrão E, Silva MT, Ferreira TR, *et al.* Impacts of land use and land cover changes on hydrological processes and sediment yield determined using the SWAT model. International Journal of Sediment Research 2022; 37(1): 54–69. doi: 10.1016/j.ijsrc.2021.04.002.
40. Admas M, Melesse AM, Abate B, Tegegne G. Soil erosion, sediment yield, and runoff modeling of the megech watershed using the GeoWEPP model. Hydrology 2022; 9(12): 208. doi: 10.3390/hydrology9120208.
41. Mekonnen YA, Mengistu TD, Asitatikie AN, Kumilachew YW. Evaluation of reservoir sedimentation using bathymetry survey: A case study on Adebra night storage reservoir, Ethiopia. Applied Water Science 2022; 12(12): 1–16. doi: 10.1007/s13201-022-01787-0.
42. Endalew L, Mulu A. Estimation of reservoir sedimentation using bathymetry survey at Shumburit earth dam, East Gojjam zone Amhara region, Ethiopia. Heliyon 2022; 8(12): e11819. doi: 10.1016/j.heliyon.2022.e11819.
43. Shrestha P, Janauer GA. Management of aquatic macrophyte resource: A case of Phewa Lake, Nepal. In: Jha PK, Baral SR, Karmacharya SB, *et al.* (editors). Environment and agriculture: Biodiversity, agriculture and pollution in South Asia. Kathmandu: Ecological Society (ECOS); 2001. p. 99–107.
44. Paudyal K, Baral H, Putzel L, *et al.* Change in land use and ecosystem services delivery from community-based forest landscape restoration in the Phewa Lake watershed, Nepal. International Forestry Review 2017; 19(4): 88–101. doi: 10.1505/146554817x15168881187636.
45. Paudyal K, Baral H, Bhandari S, *et al.* Spatial assessment of the impact of land use and land cover change on supply of ecosystem services in Phewa watershed, Nepal. Ecosystem Services 2019; 36:100895. doi: https://doi.org/10.1016/j.ecoser.2019.100895.
46. Government of Nepal (GoN)/United Nations Development Programme (UNDP). Development of ecosystem based sediment control techniques and design of siltation dam to protect Phewa lake. Government of Nepal (GoN)/United Nations Development Programme (UNDP); 2015.
47. Pant RR, Adhikari NL. Water quality assessment of Phewa Lake, Pokhara Nepal. Cognitive Transdisciplinary Research Journal 2015; 1: 130–140.
48. Leibundgut G, Sudmeier-Rieux K, Devkota S, *et al.* Rural earthen roads impact assessment in Phewa watershed, Western region, Nepal. Geoenvironmental Disasters 2016; 3(13): 1–21. doi:10.1186/s40677-016-0047-8.
49. JICA. Final report for development study on the environmental conservation of Phewa Lake in Pokhara, Nepal [Internet]. Nepal Office, Japan International Cooperation Agency: SILT Consultants (P) Ltd; 2002. Available from: http://open_jicareport.jica.go.jp/619/619/619_116_11688165.html.
50. Watson CS, Kargel JS, Regmi D, *et al.* Shrinkage of Nepal's second largest lake (Phewa Tal) due to watershed degradation and increased sediment influx. Remote Sensing 2019; 11(4): 1–17. doi: 10.3390/rs11040444.
51. Department of Soil Conservation. Sedimentation survey of Phewa Lake. Department of Soil Conservation (DSC); Research and Soil Conservation Sections; HMG Ministry of Forest and Soil Conservation: Kathmandu, Nepal, 1994; p. 1–26. Cited by: Watson CS, Kargel JS, Regmi D, *et al.* Shrinkage of Nepal's second largest lake (Phewa Tal) due to watershed degradation and increased sediment influx. Remote Sensing 2019; 11(4): 444. doi: 10.3390/rs11040444.
52. Ross J, Gilbert R. Lacustrine sedimentation in a monsoon environment: The record from Phewa Tal, middle mountain region of Nepal. Geomorphology 1999; 27(3–4): 307–323. doi:10.1016/S0169-555X(98)00079-8.
53. Sthapit KM, Balla MK. Sedimentation monitoring of Phewa Lake. Institute of Forestry/International Tropical Timber Organization; 1998.
54. Bhandari KP, Aryal J, Darnsawasdi R. A geospatial approach to assessing soil erosion in a watershed by integrating socio-economic determinants and the

RUSLE model. Natural Hazards 2015; 75(1): 321–342. doi: 10.1007/s11069-014-1321-2.
55. Strahler AN. Hypsometric (area-altitude) analysis of erosional topography. Geological Society of America Bulletin 1952; 63(11): 1117–1142. doi: 10.1130/0016-7606(1952)63[1117:HAA-OET]2.0.CO;2.
56. Horton RE. Erosional development of streams and their drainage basins; Hydrophysical approach to quantitative morphology. Geological Society of America Bulletin 1945; 56(3): 275–370. doi: 10.1130/0016-7606(1945)56[275:EDOSAT]2.0.CO;2.
57. Strahler AN. Quantitative geomorphology of drainage basins and channel networks. In: Chow V (editor). Handbook of applied hydrology. New York: McGraw Hill; 1964. p. 439–476.
58. Schumm SA. Evolution of drainage systems and slopes in badlands at Perth Amboy, New Jersey. Geological Society of America Bulletin 1956; 67(5): 597–646. doi: 10.1130/0016-7606(1956)67[597:EODSAS]2.0.CO;2.
59. Horton RE. Drainage-basin characterstics. Transactions, American Geophysical Union.1932; 13(1): 350–361. doi: 10.1029/TR013i001p00350.
60. Schumm SA, Hadley RF. Progress in the application of landform analysis in studies of semiarid erosion. Reston: U.S. Geological Survey; 1961.
61. Schumm SA. Sinuosity of alluvial rivers on the great plains. Geological Society of America Bulletin 1963; 74(9): 1089–1100. doi: 10.1130/0016-7606(1963)74[1089:SOAROT]2.0.CO;2.
62. Asfaw D, Workineh G. Quantitative analysis of morphometry on Ribb and Gumara watersheds: Implications for soil and water conservation. International Soil and Water Conservation Research 2019; 7(2): 150–157. doi: 10.1016/j.iswcr.2019.02.003.
63. Farhan Y, Anbar A, Al-Shaikh N, Mousa R. Prioritization of semi-arid agricultural watershed using morphometric and principal component analysis, remote sensing, and GIS techniques, the Zerqa River watershed, Northern Jordan. Agricultural Sciences 2017; 8: 113–148. doi: 10.4236/as.2017.81009.
64. Debelo G, Tadele K, Koriche SA. Morphometric analysis to identify erosion prone areas on the upper blue Nile using GIS (case study of Didessa and Jema Sub-Basin, Ethiopia). International Research Journal of Engineering and Technology 2017; 4(8): 1773–1784.
65. Singh P, Gupta A, Singh M. Hydrological inferences from watershed analysis for water resource management using remote sensing and GIS techniques. The Egyptian Journal of Remote Sensing and Space Science 2014; 17(2): 111–121. doi: 10.1016/j.ejrs.2014.09.003.
66. Withanage NS, Dayawansa NDK, De Silva RP. Morphometric analysis of the Gal Oya River Basin using spatial data derived from GIS. Tropical Agricultural Research 2014; 26(1): 175–188. doi: 10.4038/tar.v26i1.8082.
67. Baral P, Wen Y, Urriola N. Forest cover changes and trajectories in a typical middle mountain watershed of western Nepal. Land 2018; 7(2): 72. doi: 10.3390/land7020072.
68. Vuillez C, Tonini M, Sudmeier-Rieux K, *et al.* Land use changes, landslides and roads in the Phewa watershed, Western Nepal from 1979 to 2016. Applied Geography 2018; 94: 30–40. doi: 10.1016/j.apgeog.2018.03.003.
69. Quilbé R, Rousseau AN, Moquet JS, *et al.* Hydrological responses of a watershed to historical land use evolution and future land use scenarios under climate change conditions. Hydrology and Earth System Sciences 2008; 12(1): 101–110. doi: 10.5194/hess-12-101-2008.